MIT Open Access Articles

Source Term Study on Tritium in HTR-PM: Theoretical Calculations and Experimental Design

Research Article

Source Term Study on Tritium in HTR-PM: Theoretical Calculations and Experimental Design

Jianzhu Cao,[1] Liguo Zhang,[1] Feng Xie,[1] Bing Xia,[1] and Stephen Tsz Tang Lam[2]

[1]*Institute of Nuclear and New Energy Technology, Collaborative Innovation Center of Advanced Nuclear Energy Technology, Key Laboratory of Advanced Reactor Engineering and Safety of Ministry of Education, Tsinghua University, Beijing 100084, China*
[2]*Department of Nuclear Science and Engineering, MIT, Cambridge, MA 02139, USA*

Correspondence should be addressed to Feng Xie; fxie@tsinghua.edu.cn

The high temperature gas-cooled reactor pebble-bed module (HTR-PM) in China received much attention for its inherent safety performance and high thermal efficiency. The generation mechanism, distribution, reduction route, and release type of tritium (H-3) in HTR-PM are presented with a complete theoretical model. The calculation results indicate the majority of H-3 in the core is generated by the activation reaction of B-10. The activity concentration of H-3 in the primary loop and the specific activity of H-3 in the secondary loop at the operating equilibrium are computed as $3.69 \times 10^6\ \mathrm{Bq/m^3_{STP}}$ of helium and $4.22 \times 10^4\ \mathrm{Bq/kg}$ of water, respectively. The H-3 sampling measurement in HTR-PM has been designed to collect data from the primary coolant, from the liquid waste storage tank, from the secondary coolant, and from the liquid and gaseous effluents, separately. In this paper, the design of H-3 sampling positions in the helium purification system is discussed. The H-3 sampling measurement from the primary helium in HTR-PM has been improved, which can provide reliable activity concentration data of H-3 in the primary loop and supply accurate evaluation for the efficiency of the helium purification system.

1. Introduction

Since the radiological release of tritium (H-3) can significantly impact human health and environmental safety, the behavior of H-3 in nuclear systems is of great concern in nuclear designs. The mechanisms of H-3 generation, transport, and release in high temperature gas-cooled reactors (HTGRs) have been studied widely in several countries over the last century. Forsyth investigated the tritium production, migration, and removal in the Dragon reactor [1]. Wichner and Dyer studied the distribution and transport characteristics of tritium in the Peach Bottom HTGR [2]. Steinwarz et al. summarized the tritium behavior in the high temperature reactor according to the experience of Arbeitsgemeinschaft Versuchsreaktor (AVR) [3]. Gainey reviewed the tritium behavior in HTGR systems and concluded that tritium release was well within Federal guidelines in 1976 [4]. The regulations on tritium discharge in the effluent streams of a nuclear power plant are becoming increasingly strict. With

the development of HTGRs, research on tritium behavior gained more attention due to the significantly higher H-3 generation compared to light water reactors and higher permeation of H-3 to the secondary loop or other related systems at a high temperature. Yook et al. estimated the tritium behavior in the 300 MWth pebble-bed gas-cooled reactor for hydrogen production [5]. Ohashi et al. studied the tritium concentration numerically in the hydrogen product stream of Japan's future very high temperature gas-cooled reactor (VHTR) system coupled with a thermochemical water-splitting iodine-sulfur (IS) process [6]. Dipu et al. measured the tritium concentration in the high temperature engineering test reactor (HTTR) during high temperature (950°C) continuous operation for 50 days [7].
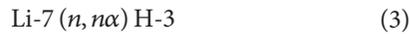
The Institute of Nuclear and New Energy Technology (INET), Tsinghua University, has led the research and development on HTGRs in China since the 1980s. The first Chinese HTGR called HTR-10, a 10 MW high temperature gas-cooled reactor, was designed and built by INET. The HTR-10 was

a helium cooled, graphite-moderated, and thermal neutron spectrum reactor [8], which achieved criticality in 2000 and ran with full power in 2003. On the basis of the technology and experience of HTR-10 and AVR, the demonstration power plant HTR-PM, a high temperature gas-cooled reactor pebble-bed module, has been designed by INET. The total thermal power and electrical output of HTR-PM, which is composed of two modules, are 500 MW and 200 MW, respectively [9]. Currently, HTR-PM is under construction in Shidao Bay, Rongcheng City, Shandong Province, China.

Xu et al. studied the source terms of tritium in HTR-10 theoretically [10]. The tritium concentration in the primary loop of HTR-10 has been measured at three different sampling positions in the helium purification system (HPS) [11]. Wu and Cao presented a preliminary analysis on tritium production and distribution in HTR-PM using predesign parameters and estimated the tritium inventory in the primary coolant and in the secondary loop but omitted the source from activation reactions of Li-7 and B-10 [12]. In this current paper, the generation, distribution, reduction, and release of H-3 in HTR-PM will be analyzed with a theoretical model in detail. The amount and proportion of H-3 from various sources in the reactor core are calculated, the variation of the activity concentration of H-3 in the primary coolant over time is modeled, the specific activity of H-3 in the secondary loop is presented and discussed, and the released amount of H-3 in gaseous, liquid, and solid waste is compared. Additionally, the experimental design for H-3 measurement in HTR-PM is introduced. The sampling positions and design of H-3 measurement in the helium purification system are discussed as well as the improvement of the sampling technology of H-3 in helium.

2. Theoretical Model and Calculation Results

2.1. Theoretical Model. The generation mechanisms of H-3 in HTGRs have been thoroughly analyzed in literature [4, 7, 10], and it has been determined that H-3 is mainly produced by ternary fission reactions in the fuel and neutron absorption reaction of light nuclides in the reactor core as follows:

$$\text{He-3} \left(n, p \right) \text{H-3} \tag{1}$$

$$\text{Li-6} \left(n, \alpha \right) \text{H-3} \tag{2}$$

$$\text{Li-7} \left(n, n\alpha \right) \text{H-3} \tag{3}$$

$$\text{B-10} \left(n, 2\alpha \right) \text{H-3} \tag{4}$$

$$\text{B-10} \left(n, \alpha \right) \text{Li-7} \tag{5}$$

In HTR-PM, ternary fissile nuclides in the fuel element are U-235, Pu-239, and Pu-241. The activation reactions of He-3 in the primary coolant in the core, Li-6 in the matrix graphite, graphite reflectors, and carbon bricks, Li-7 in the matrix graphite, graphite reflectors, absorber balls, control rods, and carbon bricks, and B-10 in absorber balls, control rods, and carbon bricks, are taken into account in the current paper. H-3 can be generated from B-10 activation reactions in two ways: directly according to (4) with fast neutrons

or indirectly according to the chain reactions of (5) with thermal neutrons and (3) with fast neutrons. Since conditions and related physical processes in the primary loop are complicated and parameters are numerous, following assumptions are made conservatively when considering the H-3 activity concentration in the primary loop of HTR-PM:

(a) H-3 will be trapped completely in the intact tristructural-isotropic (TRISO) coated particles in normal operation [13], while H-3 can be released into the primary loop from broken particles and free uranium contamination in the matrix graphite of fuel elements.

(b) Since He-3 exists in the primary coolant, all H-3 generated from the activation reaction of He-3 will enter the primary loop.

(c) All H-3 generated from activation reactions of Li-6 and Li-7 in the matrix graphite in fuel elements and graphite reflectors is thought to be released into the primary loop.

(d) Due to the low temperature (less than 400°C) in absorber balls, control rods, and carbon bricks, H-3 generated from the activation reaction of Li-6 in carbon bricks and Li-7 and B-10 in absorber balls, control rods, and carbon bricks [14, 15] are expected to be retained in situ.

(e) Absorption and diffusion processes of H-3 in the graphite and other materials inside the primary loop are not considered.

Thus, generation sources of H-3 in the primary loop include ternary fission reaction in broken particles and free uranium contamination in the matrix graphite of fuel elements, He-3 activation reaction in the primary coolant in the reactor core, and Li-6 and Li-7 activation reactions in the matrix graphite in fuel elements and graphite reflectors. As indicated by [10, 12], H-3 sinks in the primary loop of HTR-PM include leakage of the primary helium, removal in HPS, decay of H-3, and permeation of H-3 into the secondary loop. So the inventory of H-3 in the primary loop of HTR-PM can be expressed as shown in

$$\frac{dN_{\text{Tritium}}^P}{dt} = k \cdot \sum_X R_X^{\text{TF}} + R_{\text{He-3}}^{\text{PC}} + R_{\text{Li-6}}^{\text{MG}} + R_{\text{Li-6}}^{\text{GR}} + R_{\text{Li-7}}^{\text{MG}}$$
$$+ R_{\text{Li-7}}^{\text{GR}} - \left(L_p + P_{\text{ur}} + \lambda + P_{\text{er}} \right) N_{\text{Tritium}}^P, \tag{6}$$

where N_{Tritium}^P is the number of H-3 atoms in the primary loop, R_X^{TF} is the H-3 atom production rate of ternary fission reactions of nuclide X, k is the sum of the fraction of free uranium contamination and broken coated particles, $R_{\text{He-3}}^{\text{PC}}$ is the H-3 atom production rate of He-3 activation reaction in the primary coolant, $R_{\text{Li-6}}^{\text{MG}}$ and $R_{\text{Li-6}}^{\text{GR}}$ are the H-3 atom production rates of Li-6 activation reactions in the matrix graphite and graphite reflectors individually, $R_{\text{Li-7}}^{\text{MG}}$ and $R_{\text{Li-7}}^{\text{GR}}$ are the H-3 atom production rates of Li-7 activation reactions in the matrix graphite and graphite reflectors, respectively, L_p is the release rate of the helium coolant in the primary loop (s^{-1}), P_{ur} is the purification rate of the HPS (s^{-1}), λ is the decay constant of H-3 (s^{-1}), and P_{er} is the fractional permeation rate of H-3 into the secondary loop (s^{-1}).

In the following section, we will introduce the H-3 generation equations in the primary loop and H-3 activity

concentration calculations in the secondary coolant of HTR-PM. Equations (7)–(10), (12), and (13) below are used in the calculation of the primary loop tritium inventory in (6).

The H-3 generated from ternary fission reaction of the nuclide X, R_X^{TF}, can be given as

$$R_X^{\mathrm{TF}} = \frac{P_{\mathrm{th}}}{g} \cdot y_x \cdot f_x, \tag{7}$$

where P_{th} is the thermal power of the reactor (MW), g is the energy released per fission (MW·s), y_x is the average yield of H-3 production per fission of the nuclide X, and f_x is the fissile fraction of the nuclide X.

The H-3 generation rate from the activation reaction of He-3, $R_{\mathrm{He\text{-}3}}^{\mathrm{PC}}$, can be expressed as

$$
\begin{aligned}
&R_{\mathrm{He\text{-}3}}^{\mathrm{PC}} \\
&= \sigma_{\mathrm{He\text{-}3}}\phi_{\mathrm{Th}}N_{\mathrm{He\text{-}3}}^0 \\
&\cdot \left(\frac{\sigma_{\mathrm{He\text{-}3}}\phi_{\mathrm{Th}}}{L_p + \sigma_{\mathrm{He\text{-}3}}\phi_{\mathrm{Th}}} \cdot e^{-(L_p + \sigma_{\mathrm{He\text{-}3}}\phi)t} + \frac{L_p}{L_p + \sigma_{\mathrm{He\text{-}3}}\phi_{\mathrm{Th}}} \right),
\end{aligned}
\tag{8}
$$

where $\sigma_{\mathrm{He\text{-}3}}$ is the cross section of the activation reaction of He-3 (n, p) H-3 (barns), ϕ_{Th} is the average thermal neutron fluence rate in the core (cm^{-2}·s^{-1}), and $N_{\mathrm{He\text{-}3}}^0$ is the initial He-3 atoms number in the helium in the core.

The H-3 generation rate from the activation reaction of Li-6 in the matrix graphite $R_{\mathrm{Li\text{-}6}}^{\mathrm{MG}}$ can be given as

$$R_{\mathrm{Li\text{-}6}}^{\mathrm{MG}} = N_F \cdot \frac{\int_{t=0}^{t=T} \sigma_{\mathrm{Li\text{-}6}}\phi_{\mathrm{Th}}N_{\mathrm{FE\_Li\text{-}6}}^0 \cdot e^{-\sigma_{\mathrm{Li\text{-}6}}\phi_{\mathrm{Th}}t}dt}{T}, \tag{9}$$

where N_F is the number of fuel elements in the equilibrium reactor core, $\sigma_{\mathrm{Li\text{-}6}}$ is the cross section of the activation reaction of Li-6 (n, α) H-3 (barns), $N_{\mathrm{FE\_Li\text{-}6}}^0$ is the initial number of Li-6 atoms in a fresh fuel element, and T is the dwell time for a fuel element in the core which is 1,050 days for HTR-PM. The curve which was made up by the consumption of Li-6 in all fuel elements at one point was the same as that in a fuel element during 1,050 days, assuming that the distribution of the burn-up of all fuel elements in HTR-PM was continuous [16].

The H-3 generation rate from the activation reaction of Li-6 in graphite reflectors $R_{\mathrm{Li\text{-}6}}^{\mathrm{GR}}$ can be given as

$$R_{\mathrm{Li\text{-}6}}^{\mathrm{GR}} = \sigma_{\mathrm{Li\text{-}6}} \cdot \phi_{\mathrm{Th}}^{\mathrm{GR}} \cdot N_{\mathrm{GR\_Li\text{-}6}}^0 \cdot e^{-\sigma_{\mathrm{Li\text{-}6}}\phi_{\mathrm{Th}}^{\mathrm{GR}}t}, \tag{10}$$

where $\phi_{\mathrm{Th}}^{\mathrm{GR}}$ is the average thermal neutron fluence rate in graphite reflectors (cm^{-2}·s^{-1}) and $N_{\mathrm{GR\_Li\text{-}6}}^0$ is the initial number of Li-6 atoms in graphite reflectors.

The H-3 generation rate from the activation reaction of Li-6 in carbon bricks $R_{\mathrm{Li\text{-}6}}^{\mathrm{CB}}$ can be given as

$$R_{\mathrm{Li\text{-}6}}^{\mathrm{CB}} = \sigma_{\mathrm{Li\text{-}6}} \cdot \phi_{\mathrm{Th}}^{\mathrm{CB}} \cdot N_{\mathrm{CB\_Li\text{-}6}}^0 \cdot e^{-\sigma_{\mathrm{Li\text{-}6}}\phi_{\mathrm{Th}}^{\mathrm{CB}}t}, \tag{11}$$

where $\phi_{\mathrm{Th}}^{\mathrm{CB}}$ is the average thermal neutron fluence rate in carbon bricks (cm^{-2}·s^{-1}) and $N_{\mathrm{CB\_Li\text{-}6}}^0$ is the initial number of Li-6 atoms in carbon bricks.

The H-3 generation rate from the activation reaction of Li-7 in the matrix graphite $R_{\mathrm{Li\text{-}7}}^{\mathrm{MG}}$, in graphite reflectors $R_{\mathrm{Li\text{-}7}}^{\mathrm{GR}}$, and in carbon bricks $R_{\mathrm{Li\text{-}7}}^{\mathrm{CB}}$ can be calculated with

$$R_{\mathrm{Li\text{-}7}}^{\mathrm{MG}} = N_F \cdot \frac{\int_{t=0}^{t=T} \sigma_{\mathrm{Li\text{-}7}}\phi_F N_{F\_\mathrm{Li\text{-}7}}^0 \cdot e^{-\sigma_{\mathrm{Li\text{-}7}}\phi_F t}dt}{T} \tag{12}$$

$$R_{\mathrm{Li\text{-}7}}^{\mathrm{GR}} = \sigma_{\mathrm{Li\text{-}7}} \cdot \phi_F^{\mathrm{GR}} \cdot N_{\mathrm{GR\_Li\text{-}7}}^0 \cdot e^{-\sigma_{\mathrm{Li\text{-}7}}\phi_F^{\mathrm{GR}}t} \tag{13}$$

$$R_{\mathrm{Li\text{-}7}}^{\mathrm{CB}} = \sigma_{\mathrm{Li\text{-}7}} \cdot \phi_F^{\mathrm{CB}} \cdot N_{\mathrm{CB\_Li\text{-}7}}^0 \cdot e^{-\sigma_{\mathrm{Li\text{-}7}}\phi_F^{\mathrm{CB}}t}, \tag{14}$$

where $\sigma_{\mathrm{Li\text{-}7}}$ is the cross section of the activation reaction of Li-7 $(n, n\alpha)$ H-3 (barns), ϕ_F is the average fast neutron fluence rate in the core (cm^{-2}·s^{-1}), $N_{F\_\mathrm{Li\text{-}7}}^0$ is the initial number of Li-7 atoms in a fresh fuel element, ϕ_F^{GR} is the average fast neutron fluence rate in graphite reflectors (cm^{-2}·s^{-1}), $N_{\mathrm{GR\_Li\text{-}7}}^0$ is the initial number of Li-7 atoms in graphite reflectors, ϕ_F^{CB} is the average fast neutron fluence rate in carbon bricks (cm^{-2}·s^{-1}), and $N_{\mathrm{CB\_Li\text{-}7}}^0$ is the initial number of Li-7 atoms in carbon bricks.

The H-3 generation rate from the activation reaction of B-10 in carbon bricks $R_{\mathrm{B\text{-}10}}^{\mathrm{CB}}$ can be described as

$$
\begin{aligned}
R_{\mathrm{B\text{-}10}}^{\mathrm{CB}} = {}&N_{\mathrm{CB\_B\text{-}10}}^0 \\
&\times \left(\frac{\left(\sigma_{(n,2\alpha)\mathrm{B\text{-}10}}\phi_F^{\mathrm{CB}} + \sigma_{(n,\alpha)\mathrm{B\text{-}10}}\phi_{\mathrm{Th}}^{\mathrm{CB}}\right) \cdot \left(\sigma_{(n,2\alpha)\mathrm{B\text{-}10}}\phi_F^{\mathrm{CB}} - \sigma_{\mathrm{Li\text{-}7}}\phi_F^{\mathrm{CB}}\right)}{\sigma_{(n,2\alpha)\mathrm{B\text{-}10}}\phi_F^{\mathrm{CB}} + \sigma_{(n,\alpha)\mathrm{B\text{-}10}}\phi_{\mathrm{Th}}^{\mathrm{CB}} - \sigma_{\mathrm{Li\text{-}7}}\phi_F^{\mathrm{CB}}} \right. \\
&\times e^{-(\sigma_{(n,2\alpha)\mathrm{B\text{-}10}}\phi_F^{\mathrm{CB}} + \sigma_{(n,\alpha)\mathrm{B\text{-}10}}\phi_{\mathrm{Th}}^{\mathrm{CB}})t} \\
&\left. + \frac{\sigma_{(n,\alpha)\mathrm{B\text{-}10}}\phi_{\mathrm{Th}}^{\mathrm{CB}} \cdot \sigma_{\mathrm{Li\text{-}7}}\phi_F^{\mathrm{CB}}}{\sigma_{(n,2\alpha)\mathrm{B\text{-}10}}\phi_F^{\mathrm{CB}} + \sigma_{(n,\alpha)\mathrm{B\text{-}10}}\phi_{\mathrm{Th}}^{\mathrm{CB}} - \sigma_{\mathrm{Li\text{-}7}}\phi_F^{\mathrm{CB}}} \times e^{-\sigma_{\mathrm{Li\text{-}7}}\phi_F^{\mathrm{CB}}t} \right),
\end{aligned}
\tag{15}
$$

where $N_{\mathrm{CB\_B\text{-}10}}^0$ is the initial number of B-10 atoms in carbon bricks, $\sigma_{(n,2\alpha)\mathrm{B\text{-}10}}$ is the cross section of the activation reaction of B-10 $(n, 2\alpha)$ H-3 (barns), and $\sigma_{(n,\alpha)\mathrm{B\text{-}10}}$ is the cross section of the activation reaction of B-10 (n, α) Li-7 (barns).

Similarly, the H-3 generation rate from the activation reaction of B-10 in absorber balls $R_{\mathrm{B\text{-}10}}^{\mathrm{AB}}$ and in control rods $R_{\mathrm{B\text{-}10}}^{\mathrm{CR}}$ can be described with the corresponding average thermal neutron fluence rate, average fast neutron fluence rate, and number of B-10 atoms as shown:

$$
\begin{aligned}
R_{\mathrm{B\text{-}10}}^{\mathrm{AB}} = {}&N_{\mathrm{AB\_B\text{-}10}}^0 \\
&\times \left(\frac{\left(\sigma_{(n,2\alpha)\mathrm{B\text{-}10}}\phi_F^{\mathrm{AB}} + \sigma_{(n,\alpha)\mathrm{B\text{-}10}}\phi_{\mathrm{Th}}^{\mathrm{AB}}\right) \cdot \left(\sigma_{(n,2\alpha)\mathrm{B\text{-}10}}\phi_F^{\mathrm{AB}} - \sigma_{\mathrm{Li\text{-}7}}\phi_F^{\mathrm{AB}}\right)}{\sigma_{(n,2\alpha)\mathrm{B\text{-}10}}\phi_F^{\mathrm{AB}} + \sigma_{(n,\alpha)\mathrm{B\text{-}10}}\phi_{\mathrm{Th}}^{\mathrm{AB}} - \sigma_{\mathrm{Li\text{-}7}}\phi_F^{\mathrm{AB}}} \right. \\
&\times e^{-(\sigma_{(n,2\alpha)\mathrm{B\text{-}10}}\phi_F^{\mathrm{AB}} + \sigma_{(n,\alpha)\mathrm{B\text{-}10}}\phi_{\mathrm{Th}}^{\mathrm{AB}})t} \\
&\left. + \frac{\sigma_{(n,\alpha)\mathrm{B\text{-}10}}\phi_{\mathrm{Th}}^{\mathrm{AB}} \cdot \sigma_{\mathrm{Li\text{-}7}}\phi_F^{\mathrm{AB}}}{\sigma_{(n,2\alpha)\mathrm{B\text{-}10}}\phi_F^{\mathrm{AB}} + \sigma_{(n,\alpha)\mathrm{B\text{-}10}}\phi_{\mathrm{Th}}^{\mathrm{AB}} - \sigma_{\mathrm{Li\text{-}7}}\phi_F^{\mathrm{AB}}} \times e^{-\sigma_{\mathrm{Li\text{-}7}}\phi_F^{\mathrm{AB}}t} \right) \\
R_{\mathrm{B\text{-}10}}^{\mathrm{CR}} = {}&N_{\mathrm{CR\_B\text{-}10}}^0 \\
&\times \left(\frac{\left(\sigma_{(n,2\alpha)\mathrm{B\text{-}10}}\phi_F^{\mathrm{CR}} + \sigma_{(n,\alpha)\mathrm{B\text{-}10}}\phi_{\mathrm{Th}}^{\mathrm{CR}}\right) \cdot \left(\sigma_{(n,2\alpha)\mathrm{B\text{-}10}}\phi_F^{\mathrm{CR}} - \sigma_{\mathrm{Li\text{-}7}}\phi_F^{\mathrm{CR}}\right)}{\sigma_{(n,2\alpha)\mathrm{B\text{-}10}}\phi_F^{\mathrm{CR}} + \sigma_{(n,\alpha)\mathrm{B\text{-}10}}\phi_{\mathrm{Th}}^{\mathrm{CR}} - \sigma_{\mathrm{Li\text{-}7}}\phi_F^{\mathrm{CR}}} \right.
\end{aligned}
$$
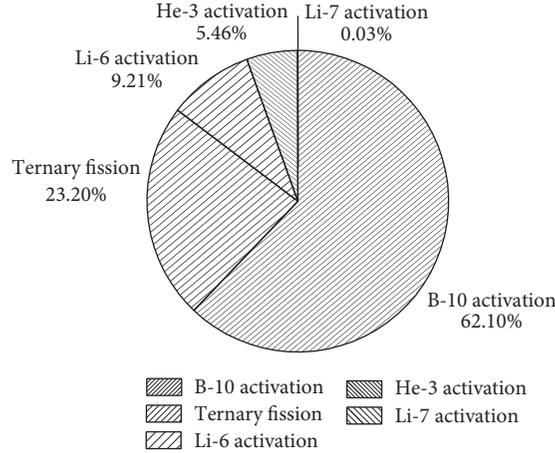
FIGURE 1: Fraction of H-3 generation amount in the reactor core from various sources in HTR-PM.

$$\times e^{-(\sigma_{(n,2\alpha)\text{B-10}}\phi_F^{\text{CR}}+\sigma_{(n,\alpha)\text{B-10}}\phi_{\text{Th}}^{\text{CR}})t}$$

$$+ \frac{\sigma_{(n,\alpha)\text{B-10}}\phi_{\text{Th}}^{\text{CR}} \cdot \sigma_{\text{Li-7}}\phi_F^{\text{CR}}}{\sigma_{(n,2\alpha)\text{B-10}}\phi_F^{\text{CR}}+\sigma_{(n,\alpha)\text{B-10}}\phi_{\text{Th}}^{\text{CR}}-\sigma_{\text{Li-7}}\phi_F^{\text{CR}}} \times e^{-\sigma_{\text{Li-7}}\phi_F^{\text{CR}}t}\Bigg),$$

$$(16)$$

where $N_{\text{AB\_B-10}}^0$ and $N_{\text{CR\_B-10}}^0$ are the initial number of B-10 atoms in absorbed balls and control rods separately, ϕ_F^{AB} and ϕ_F^{CR} are the average thermal neutron fluence rate in absorbed balls and control rods ($\text{cm}^{-2}\cdot\text{s}^{-1}$) individually, and ϕ_F^{AB} and ϕ_F^{CR} are the average fast neutron fluence rate in absorbed balls and control rods ($\text{cm}^{-2}\cdot\text{s}^{-1}$), respectively. The derivation of (8), (9), and (15) can be found in [10].

The H-3 can permeate through the heat exchange tubes in the steam generator from the primary loop at high temperatures in HTGRs, which will be the only source term in the secondary loop. Considering the leakage of the water in the secondary loop and the decay of H-3, the tritium inventory in the secondary loop can be calculated as

$$\frac{dN_{\text{Tritium}}^S}{dt} = P_{\text{er}} \cdot N_{\text{Tritium}}^P - (L_s + \lambda) \cdot N_{\text{Tritium}}^S, \qquad (17)$$

where N_{Tritium}^S is the number of H-3 atoms in the secondary loop and L_s is the fractional leakage rate of water in the secondary loop (s^{-1}).

2.2. Dominant Parameters. The dominant parameters are listed in Table 1 for each module of HTR-PM, most of which are cited from the Final Safety Analysis Report of HTR-PM [17].

2.3. Calculation Results. Using (7)–(16), the production of H-3 in the reactor core components of HTR-PM during 40 years' operation can be calculated as listed in Table 2. The activation of B-10 in control rods, ternary fission reaction in fuel elements, and the activation of Li-6 in fuel elements are the first three main generation sources of H-3 in HTR-PM. Compared to Li-6, the production amount of H-3

from Li-7 activation is two orders of magnitude lower as indicated in Figure 1. In the primary loop, the dominant contribution of H-3 comes from Li-6 activation reaction in the matrix graphite, which accounts for about 50% of the total production in the primary loop. He-3 activation reaction is also an important source term of H-3 in the primary loop, which accounts for 37% of production as indicated in Figure 2. Although ternary fission reaction can produce a large amount of H-3 in the reactor core, most of H-3 is trapped in the intact TRISO coated particles and only a very small percentage of H-3 can be released into the primary loop.

Figure 3 indicates the variation of activity concentration of H-3 in the primary loop in HTR-PM during the 40-year lifetime. Due to activation reactions of He-3 in the helium in the reactor core and Li-6 in the matrix graphite and graphite reflectors at the initial start of HTR-PM, the activity concentration of H-3 in the primary loop increases rapidly to the maximum value of $2.83 \times 10^7\,\text{Bq/m}^3_{\text{STP}}$. However, with the purification of the helium purification system, the permeation to the secondary loop, the leakage of the primary coolant, and the decay of H-3, the activity concentration of H-3 in the primary loop decreases gradually and reaches an equilibrium state at about 15 years. At the end of 40 years' operation of HTR-PM, the activity concentration of H-3 in the primary loop is $3.69 \times 10^6\,\text{Bq/m}^3_{\text{STP}}$, and the total inventory of H-3 in the primary loop of HTR-PM is $5.79 \times 10^{10}\,\text{Bq}$.

The sum of H-3 loss terms in the primary loop in HTR-PM during 40 years' operation was calculated to $1.24 \times 10^{15}\,\text{Bq}$. Figure 4 indicates the purification of HPS will make the greatest contribution in the H-3 reduction in the primary loop. The permeation of H-3 to the secondary loop through the heat exchange tubes in the steam generator accounts for approximately 6.78%, and leakage of H-3 with primary coolant and decay of H-3 account for less than 1% of total losses.

To classify waste in the HTR-PM, a similar method to that of the HTR-10 was used. The release type of H-3 has been identified into tritiated solid waste, tritiated first-class liquid waste, tritiated second-class liquid waste, and tritiated gaseous waste. The tritiated solid waste includes spent fuel

TABLE 1: Main parameters used in the calculation of H-3 in HTR-PM.

Parameter	Design value
Rated thermal power for each module of HTR-PM	250 MW
Average thermal neutron fluence rate in the reactor core	$7.10E + 13\,\text{cm}^{-2}\cdot\text{s}^{-1}$
Average thermal neutron fluence rate in graphite reflectors	$2.70E + 13\,\text{cm}^{-2}\cdot\text{s}^{-1}$
Average fast fluence rate in graphite reflectors	$4.10E + 12\,\text{cm}^{-2}\cdot\text{s}^{-1}$
Average thermal neutron fluence rate in control rods	$2.45E + 13\,\text{cm}^{-2}\cdot\text{s}^{-1}$
Average fast neutron fluence rate in control rods	$4.10E + 12\,\text{cm}^{-2}\cdot\text{s}^{-1}$
Average thermal neutron fluence rate in absorber balls	$2.49E + 10\,\text{cm}^{-2}\cdot\text{s}^{-1}$
Average fast neutron fluence rate in absorber balls	$2.10E + 8\,\text{cm}^{-2}\cdot\text{s}^{-1}$
Average thermal neutron fluence rate in carbon bricks	$4.87E + 10\,\text{cm}^{-2}\cdot\text{s}^{-1}$
Average fast neutron fluence rate in carbon bricks	$5.86E + 8\,\text{cm}^{-2}\cdot\text{s}^{-1}$
Sum of the breakage rate and free uranium fraction	$2.61E - 4$
Fission fraction of U-235	0.655
Fission fraction of Pu-239	0.271
Fission fraction of Pu-241	0.070
Average yield of H-3 production per fission of U-235	$8.00E - 5$
Average yield of H-3 production per fission of Pu-239	$1.80E - 4$
Average yield of H-3 production per fission of Pu-241	$1.50E - 4$
Helium volume in the primary loop	15,690 Nm^3
He-3 abundance in the primary helium	$1.40E - 7$
Mass of matrix graphite of each fuel element	0.186 kg
Li abundance in matrix graphite, graphite reflectors, and carbon bricks	0.05 ppm
Mass of graphite reflectors	252,000 kg
Mass of carbon bricks	128,000 kg
Mass of B_4C in absorber balls	231 kg
Mass of B_4C in control rods	1,877 kg
Content of B_4C in carbon bricks	5%
Fractional leakage rate of the primary coolant	0.5%/d
Fractional purification rate of HPS	5%/h
Fractional permeation rate of H-3 to the secondary loop	0.365%/h
Mass of water in the secondary loop	100,000 kg
Fractional leakage rate of the secondary coolant	5%/h

TABLE 2: Production amount of H-3 in the reactor core of HTR-PM during 40 years' operation.

| Source	Activity (Bq)	Proportion
Ternary fission reaction in fuel elements	$1.97E + 15$	23.20%
Activation reaction of He-3 in the primary coolant	$4.64E + 14$	5.46%
Activation reaction of Li-6 in fuel elements	$6.31E + 14$	7.43%
Activation reaction of Li-7 in fuel elements	$9.44E + 11$	0.01%
Activation reaction of Li-6 in graphite reflectors	$1.47E + 14$	1.73%
Activation reaction of Li-7 in graphite reflectors	$1.40E + 12$	0.02%
Activation reaction of Li-6 in carbon bricks	$4.19E + 12$	0.05%
Activation reaction of Li-7 in carbon bricks	$1.02E + 08$	0.00%
Activation reaction of B-10 in carbon bricks	$1.89E + 13$	0.22%
Activation reaction of B-10 in control rods	$5.26E + 15$	61.88%
Activation reaction of B-10 in absorber balls	$4.95E + 10$	0.00%
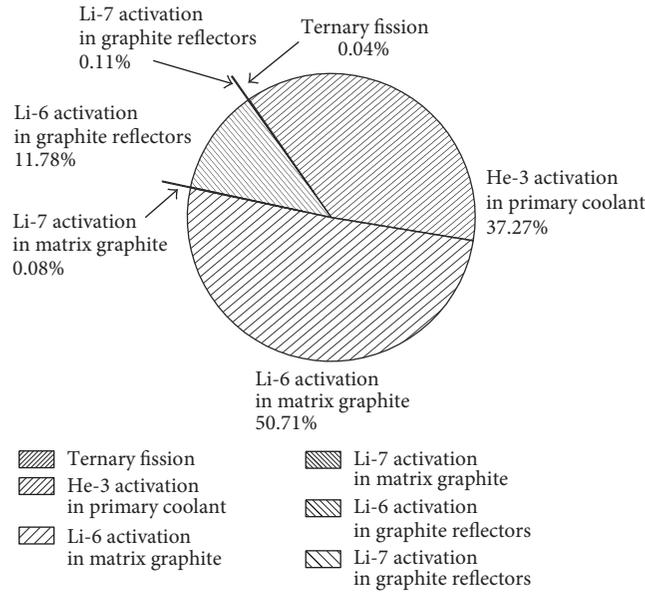
FIGURE 2: Fraction of H-3 generation amount in the primary coolant from various sources in HTR-PM.
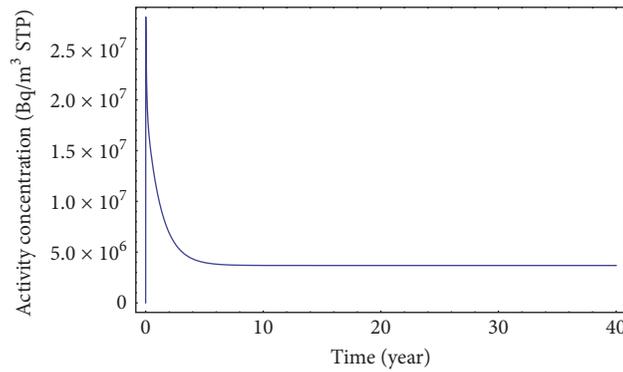

FIGURE 3: Variation of activity concentration of H-3 in the primary loop in HTR-PM during 40 years' operation.
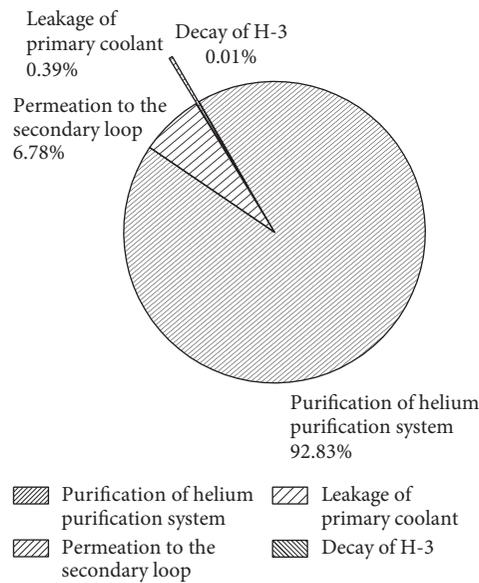

FIGURE 4: Fraction of H-3 reduction of various routes from the primary loop in HTR-PM during 40 years' operation.
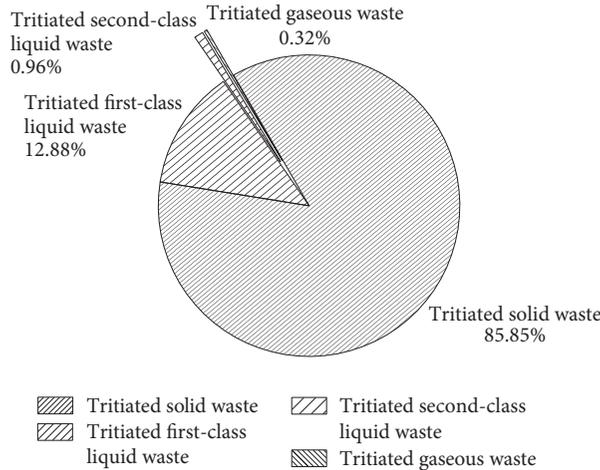
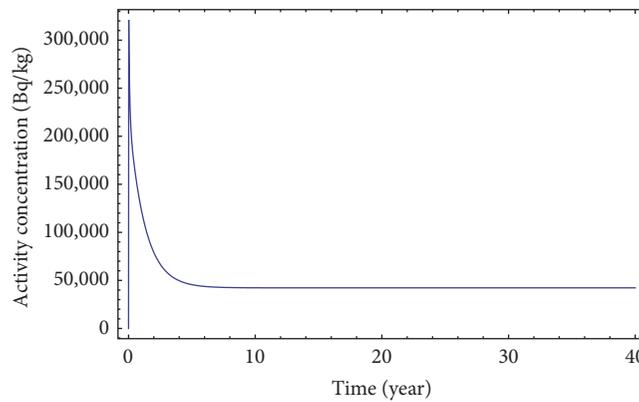FIGURE 5: Fraction of H-3 in different release types annually in HTR-PM.

FIGURE 6: Variation of the specific activity of H-3 in the secondary loop in HTR-PM during 40 years' operation.

elements, graphite reflectors, absorber balls, control rods, and carbon bricks. The tritiated first-class liquid waste is estimated with the assumption that 98% of H-3 from the purification of HPS was retained during the regeneration and desorption process of the molecular sieve adsorber. The tritiated second-class liquid waste is produced from the leakage of the secondary water. The tritiated gaseous waste comes from the leakage of the primary coolant and exhaust gas during the regeneration process of the molecular sieve adsorber in HPS. The total tritiated annual waste in HTR-PM was about 2.20×10^{14} Bq. Figure 5 shows that tritiated solid waste accounts for about 86% of the total radioactivity with the remainder predominately accounted for by tritiated liquid waste. The tritiated first-class liquid waste will be stored in tanks, while the second-class liquid waste will be discharged under continuous radiation monitoring.

Figure 6 shows the variation of specific activity of H-3 in the secondary loop in HTR-PM during 40 years' operation, which exhibits a similar trend as that of the activity concentration of H-3 in the primary loop. This can be explained by the fact that the permeation of the H-3 from the primary loop through the heat exchanger tubes is the only source term of H-3 in the secondary loop. The maximum specific activity of

H-3 in the secondary loop can reach 3.21×10^5 Bq/kg. At the end of 40-year lifetime of HTR-PM, the specific activity of H-3 in the secondary loop is 4.22×10^4 Bq/kg, and the total inventory of H-3 in the secondary loop of HTR-PM is 4.22×10^9 Bq.

3. Experimental Design of Tritium Measurement in HTR-PM

Since H-3 is an important nuclide in the source term analysis and environmental impact assessment of nuclear power plants, much attention has been paid to the design of the H-3 sampling and monitoring systems of HTR-PM. These systems include the experimental sampling and measurement of H-3 from the primary coolant, from tritiated water in HPS, from secondary water, from the liquid effluent, and from the gaseous effluent. In this part, we will focus on the design of experimental measurement of H-3 from the primary coolant.

Figure 7 shows the schematic diagram of H-3 sampling and measurement from the primary coolant in the HPS of HTR-PM. The sampling pipes are connected into the main loop of the normal line of the HPS. The purpose and functions of HPS in HTGRs have been outlined elsewhere [18].
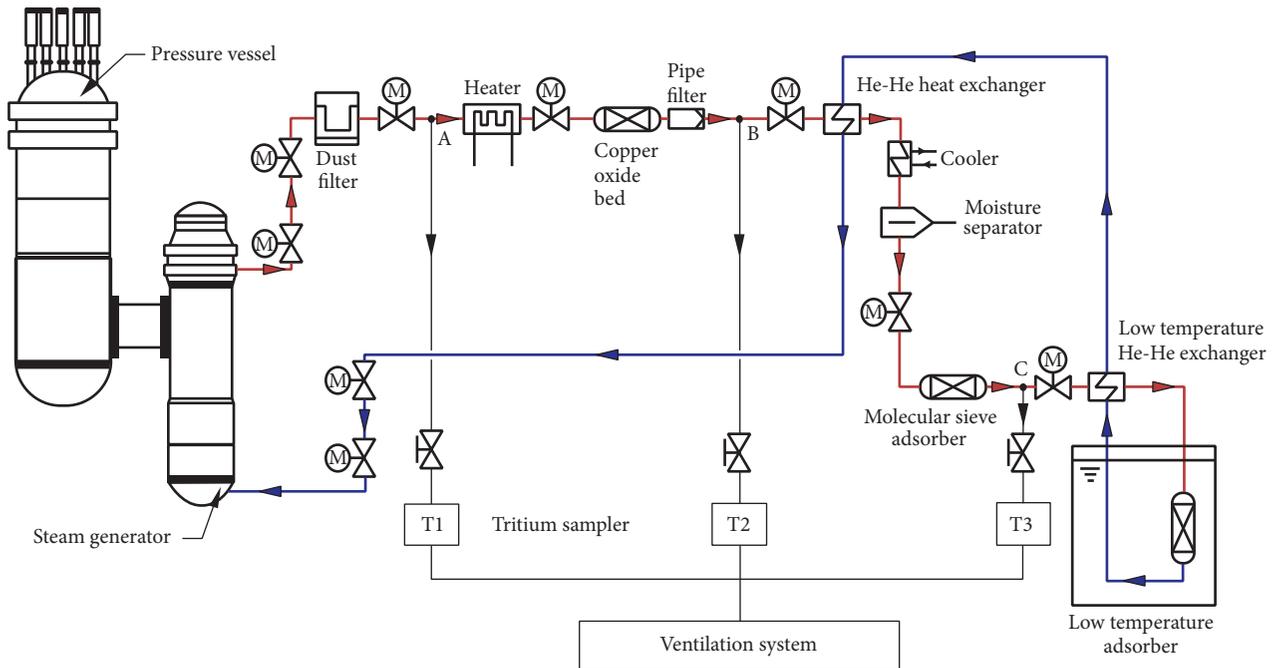
FIGURE 7: Schematic diagram of the helium purification system and tritium sampling positions in HTR-PM.

In short, the HPS can reduce chemical impurities in the primary helium, such as hydrogen, carbon monoxide, carbon dioxide, water vapor, oxygen, nitrogen, and methane, and remove the radioactive dust and gaseous fission and activation products in the primary loop, such as krypton, xenon, and tritium, to maintain the quality of the primary helium. The main components of an HPS line in HTR-PM includes a dust filter, a heater, a copper oxide bed, a pipe filter, several heat exchangers, a molecular sieve adsorber, and a low temperature adsorber. The HPS purifies a bypass coolant line at a rate of 5% of total primary helium per hour, of which the design temperature and pressure at the entrance are 250°C and 7.0 MPa, respectively.

The sampling positions of H-3 in HPS of HTR-PM are marked as sampling points A, B, and C, corresponding to the positions at the entrance of the HPS after the dust filter, at the outlet of the copper oxide bed, and at the outlet of the molecular sieve adsorber, respectively. After reducing the temperature and pressure and decreasing the flow rate, the primary helium can go through three tritium samplers T1, T2, and T3. By measuring helium flow and the activity of tritium in the sample, the activity concentration of H-3 at the corresponding sampling point can be deduced.

A part of primary helium will be purified by HPS during normal operation of HTR-PM. In the first part of this process, the radioactive dust in the helium will be retained by the dust filter. The sintered stainless powder filter tubes will be installed in this filter, which can remove solid particles of >5 μm diameter with a filtration efficiency higher than 98%. The H-3 in the gaseous form, mostly HT and HTO, with other gaseous fission and activation products, can pass through the dust filter. Thus, the sampling gas at sampling point A can reflect the gaseous composition in the primary loop.

After the dust filter, the helium will be heated by the electrical heater and flown to the copper oxide bed. The copper oxide bed will oxidize the H_2, HT, and T_2 into H_2O, HTO, and T_2O, respectively. Therefore, if oxidation efficiency of the copper oxide bed is sufficiently high, the sampled gas at sampling point B would be primarily H-3 oxide.

After oxidation in the copper oxide bed, the helium will cool down and then enter the molecular sieve adsorber to adsorb the water including H_2O, HTO, and T_2O, before reaching sampling point C, which should have very little H-3.

The activity concentration of H-3 in the primary helium can be determined with the measurement of the sampling gas from sampling point A. By comparing the activity concentration of H-3 at sampling point A with that of sampling point B, the oxidation efficiency of the copper oxide bed can be estimated. By comparing the activity concentration of H-3 at sampling point B with that of sampling point C, the adsorption efficiency of the molecular sieve adsorber can be deduced.

The tritium samplers in HTR-PM were improved upon the MARC 3000 samplers from SDEC France, by adding the air mixing module before gathering the tritium from gas into liquid sample with the bubbling technology. Figure 8 shows the schematic diagram of the tritium sampler. In the air mixing module, there are two separate lines for the primary helium and air. These lines flow into the mixing chamber with a preset mixing proportion. Without introducing oxygen, only H-3 in HTO or T_2O form can be gathered in the traditional sampler. As the air mixing module mixes the sampling gas with the air to supply a mass of oxygen, the H-3 in HT or T_2 will react to form HTO or T_2O, which can be measured to determine the original HT and T_2 in the sample stream.
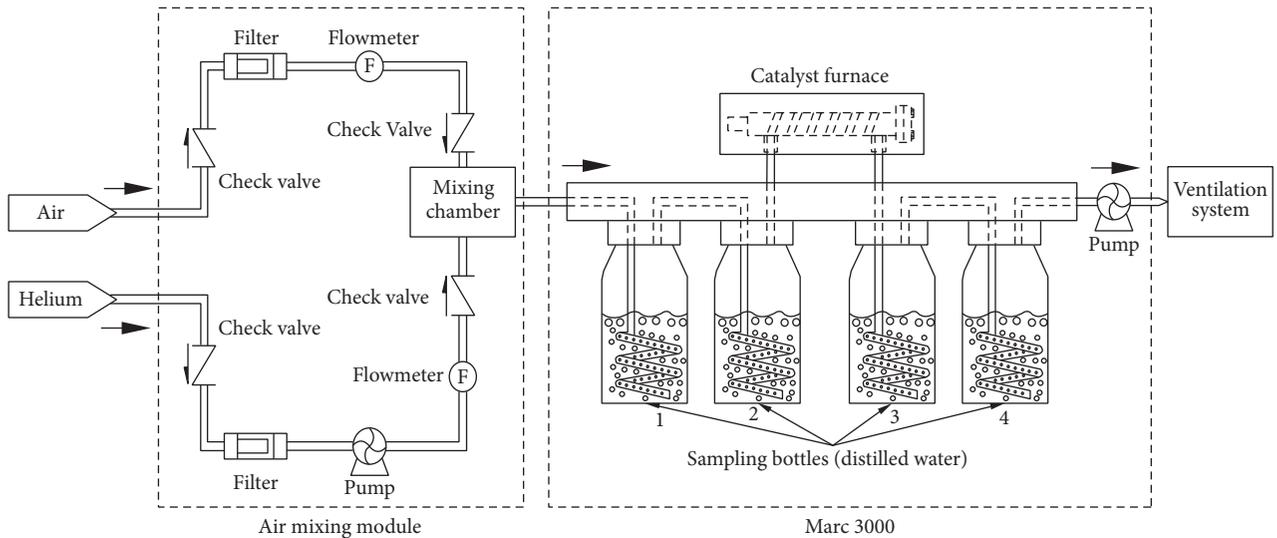
FIGURE 8: Schematic diagram of the tritium sampler adopted in HTR-PM.

The details of sampling techniques of tritium samplers can be found in [19]. The measurement techniques of the tritium with a liquid scintillation counter can be found in [20].

4. Discussions

H-3 has become a topic with common research interest not only in fission reactors but also in fusion reactors where large amounts of H-3 are generated and used as fuel [16, 21–23]. Since exposure to H-3 has long term radiological effects on personnel health and environmental safety, it is a key nuclide in the evaluation of radiation safety for nuclear facilities. In the Chinese National Standard GB6249-2011 [24], the constraints of H-3 emission via liquid and gaseous effluents for each light water reactor are 7.5×10^{13} Bq/a and 1.5×10^{13} Bq/a, respectively. In HTR-PM, a conservative estimate of the discharged amount of H-3 via liquid and gaseous effluents is 2.11×10^{12} Bq/a and 6.97×10^{11} Bq/a, respectively. These values are at least one order less than regulation limits.

However, from current calculations, a large quantity of H-3 will be left as solid waste, including spent fuel elements, graphite reflectors, absorber balls, control rods, and carbon bricks. Thus, residual solid waste will be an important issue for the decommissioning work of HTGRs. Experimental research on H-3 in the irradiated graphite spheres of HTR-10 has been conducted which can supply related information [25]. Current results indicate that most H-3 in the reactor core is generated by the activation reaction of B-10 while most H-3 in the primary coolant comes from activation reactions of He-3 and Li-6. Therefore, decreasing He-3 in the helium and Li impurity in the graphite will effectively reduce the activity concentration of H-3 in the primary coolant and consequently the specific activity of H-3 in the secondary loop.

By now, the activity concentration of H-3 in the primary loop has been determined experimentally in AVR, HTTR, and HTR-10 [7, 26]. The H-3 measurement systems in HTR-PM were enhanced based on the experience and technology developed in pressurized water reactors (PWRs) and HTR-10. Several channels have been designed for H-3 sampling and measurement from the primary coolant, from tritiated water in HPS, from secondary water, and from the liquid and gaseous effluents in HTR-PM.

Compared to the H-3 measurement from the primary loop in HTR-10, the tritium sampler of HTR-PM was improved by adding the air mixing module, which can effectively capture tritium not only in the form of HTO and T_2O but also in the form of HT and T_2. This also enables determination of the ratio of various chemical forms H-3 in the primary loop. The primary helium of HTR-PM can be sampled from sampling points A, B, and C simultaneously, which can provide a more accurate evaluation of the oxidation efficiency of the oxide copper bed and absorption efficiency of the molecular sieve adsorber and thus the purification efficiency of HPS on H-3.

The release behavior of tritium from the fuel element of HTGRs is a very important research topic. There are a few theoretical and experimental works on the absorption and diffusion processes of tritium in HTGRs [1–4, 7, 15, 16, 27]. The degree of tritium release depends on the burn-up and temperature of the fuel element. The TRISO coated particles exhibit much better tritium retention ability than that of the BISO coated particles [4]. The irradiation qualification of the HTR-PM fuel pebble has been performed in the High Flux Reactor in Petten, Netherlands [28]. Unfortunately, the fission products of Krypton and Xenon isotopes have been measured, but tritium was not included. In the Final Safety Analysis Report of HTR-PM, there are some theoretical descriptions of accident scenarios of HTR-PM [18]. However, we will use the experimental system designed in the current article to obtain the tritium concentration in the primary loop when HTR-PM is operated. Based on the experimental data in different operational stages of the reactor, we can analyze the release behavior of tritium in HTR-PM accurately and reliably.

5. Conclusion

The source term analysis of H-3 in HTR-PM has been presented with a comprehensive theoretical calculation. The calculation results indicate the overwhelming majority of H-3 in HTR-PM was produced by the activation reaction of B-10 in the reactor core. However, H-3 from this source would be retained in control rods, absorber balls, and carbon bricks. In the primary loop, most H-3 was generated by Li-6 activation in the matrix graphite and He-3 activation in the helium. At the initial start of HTR-PM, the activity concentration of H-3 in the primary loop increases rapidly to the maximum value of 2.83×10^7 Bq/m$^3_{STP}$ and reaches an equilibrium state with the value of 3.69×10^6 Bq/m$^3_{STP}$ at about 15 years. The specific activity of H-3 in the secondary loop will be 4.22×10^4 Bq/kg at the end of 40 years' operation of HTR-PM. The discharge amounts of H-3 via liquid and gaseous effluents are conservatively estimated as 2.11×10^{12} Bq/a and 6.97×10^{11} Bq/a, respectively, which satisfies the Chinese National Standard.

Based on the source term analysis of H-3 in HTR-PM and the experience of H-3 measurement in HTR-10, the experimental measurement of H-3 from the primary coolant, from tritiated water in HPS, from the secondary water, from the liquid effluent, and from the gaseous effluent in HTR-PM has been designed. The H-3 sampling measurement from the primary helium has been improved which can gather H-3 in the primary helium at different sampling points simultaneously and capture H-3 in chemical forms of HT, T$_2$, HTO, and T$_2$O. Current research results can shed a light for further theoretical and experimental study on H-3 in HTR-PM and supply important information for the decommissioning and waste minimization work in HTGRs.

Conflicts of Interest

The authors declare that they have no conflicts of interest.

Acknowledgments

References

[1] N. Forsyth, "Tritium production and distribution in high temperature gas cooled reactors part 1: tritium production, migration and removal in the dragon reactor between core 5 charge III and core 1 charge IV," O. E. C. D. High Temperature Reactor Project DRAGON DP-REPORT-799, 1972.

[2] R. P. Wichner and F. F. Dyer, "Distribution and transport of tritium in the Peach Bottom HTGR," Tech. Rep. ORNL-5497, Oak Ridge National Laboratory, Oak Ridge, TN, USA, 1979.

[3] W. Steinwarz, H. D. Röhrig, and R. Nieder, "Tritium behavior in an HTR-system based on AVR-experience," in *Specialists Meeting on Coolant Chemistry, Plate-Out and Decontamination in Gas-Cooled Reactors (IWGGCR-2)*, pp. 153–160, 1980.

[4] B. W. Gainey, "Review of tritium behavior in HTGR systems," SciTech Connect GA-A-13461, General Atomic Company, 1976.

[5] D. Yook, K. J. Lee, Y. Lee, and D. Hong, "Estimation of the tritium behavior in the pebble type gas cooled reactor for hydrogen production," *Journal of Nuclear Science and Technology*, vol. 43, no. 12, pp. 1522–1529, 2006.

[6] H. Ohashi, N. Sakaba, T. Nishihara, Y. Tachibana, and K. Kunitomi, "Analysis of tritium behavior in very high temperature gas-cooled reactor coupled with thermochemical iodine-sulfur process for hydrogen production," *Journal of Nuclear Science and Technology*, vol. 45, no. 11, pp. 1215–1227, 2008.

[7] A. L. Dipu, H. Ohashi, S. Hamamoto, H. Sato, and T. Nishihara, "Assessment of amount and concentration of tritium in HTTR-IS system based on tritium behavior during high-temperature continuous operation of HTTR," *Annals of Nuclear Energy*, vol. 88, pp. 126–134, 2016.

[8] Z. Wu, D. Lin, and D. Zhong, "The design features of the HTR-10," *Nuclear Engineering and Design*, vol. 218, pp. 25–32, 2002.

[9] Z. Zhang, Z. Wu, D. Wang et al., "Current status and technical description of Chinese 2×250 MW$_{th}$ HTR-PM demonstration plant," *Nuclear Engineering and Design*, vol. 239, no. 7, pp. 1212–1219, 2009.

[10] Y. Xu, H. Li, F. Xie, J. Cao, and J. Tong, "Source term analysis of tritium in HTR-10," *Fusion Science and Technology*, vol. 71, pp. 671–678, 2017.

[11] L. Wei, F. Xie, X. Chen, T. Ma, J. Tong, and F. Li, "Summary and experience feedback on the restart and power operation after a long-time shutdown of HTR-10," in *Proceedings of the 8th International Topical Meeting on High Temperature Reactor Technology (HTR '16)*, Las Vegas, NV, USA, November 2016.

[12] Y. Wu and J. Cao, "Analysis of tritium production and distribution in HTR-PM," in *Proceedings of the 18th International Conference on Nuclear Engineering, ICONE18*, Xian, China, May 2010.

[13] G. H. Lohnert, H. Nabielek, and W. Schenk, "The fuel element of the HTR-module, a prerequisite of an inherently safe reactor," *Nuclear Engineering and Design*, vol. 109, no. 1-2, pp. 257–263, 1988.

[14] C. C. Miles, S. Wexler, and E. R. Ebersole, "Tritium retention in EBR-II-irradiated boron carbide," SciTech Connect ANL-8107, Argonne National Laboratory, Lemont, IL, USA, 1974.

[15] T. V. Tsetskhladze, L. I. Cherkezishvili, and L. A. Chikhladze, "Interaction of tritium with graphite," *Soviet Atomic Energy*, vol. 64, no. 3, pp. 254–258, 1988.

[16] W. Steinwarz, "Tritium in HTR Plants," Tech. Rep. ISSN 0366-0855, Juelich Research Centre, Jülich, Germany, 1987.

[17] Z. Zhang, Y. Dong, and J. Huang, *Final Safety Analysis Report of the high temperature gas-cooled reactor pebble-bed module (HTR-PM)*, Institute of Nuclear and New Energy Technology, Tsinghua University, Beijing, China, 2016.

[18] M. S. Yao, R. P. Wang, Z. Y. Liu, X. D. He, and J. Li, "The helium purification system of the HTR-10," *Nuclear Engineering and Design*, vol. 218, no. 1-3, pp. 163–167, 2002.

[19] "Operating manual of tritium sampler, SDEC France," http://www.sdec-france.com/.

[20] X.-G. Feng, Q.-G. He, J.-C. Wang, and J. Chen, "The effect of sample stability on the determination of radioactivity for

various radionuclides by liquid scintillation counting," *Applied Radiation and Isotopes*, vol. 104, pp. 147–154, 2015.

[21] H. Ohashi and S. R. Sherman, "Tritium movement and accumulation in the NGNP system interface and hydrogen plant," Tech. Rep. INL/EXT-07-12746, Idaho National Laboratory, Idaho Falls, Idaho, USA, 2007.

[22] R. G. Aghoyeh and H. Khalafi, "Evaluation of tritium and Carbon-14 radioactivity in primary loop of Tehran Research Reactor (TRR)," *Progress in Nuclear Energy*, vol. 60, pp. 135–139, 2012.

[23] C. W. Forsberg, S. Lam, D. M. Carpenter, and D. G. Whyte, "Tritium control and capture in salt-cooled fission and fusion reactors: status, challenges, and path forward," *Nuclear Technology*, vol. 197, no. 2, pp. 119–139, 2017.

[24] Ministry of Environment Protection of China, "Regulations for environmental radiation protection of nuclear power plant," Tech. Rep. GB 6249-2011, 2011.

[25] X. Liu, X. Huang, F. Xie, F. Jia, X. Feng, and H. Li, "Source term analysis of irradiated graphite in the core of HTR-10," *Science and Technology of Nuclear Installations*, vol. 2017, Article ID 2614890, 6 pages, 2017.

[26] R. Bäumer and H. Barnert, *AVR-Experimental High-Temperature Reactor: 21 Years of Successful Operation for a Future Energy Technology*, The Association of German Engineers (VDI-Verlag GmbH), Düsseldorf, Germany, 1990.

[27] H. D. Röhrig, P. G. Fischer, and R. Hecker, "Tritium balance in high-temperature gas-cooled reactors," *Journal of the American Ceramic Society*, vol. 59, no. 7-8, pp. 316–320, 1976.

[28] S. Knol, S. de Groot, R. V. Salama et al., "HTR-PM fuel pebble irradiation qualification in the high flux reactor in Petten," in *Proceedings of the 8th International Topical Meeting on High Temperature Reactor Technology (HTR '16)*, Las Vegas, NV, USA, November 2016.